# Time-Resolved Optical Absorption Studies of Intramolecular Electron Transfer in Cytochrome *c* Oxidase†

Katy E. Georgiadis, Nam-In Jhon, and Ólöf Einarsdóttir*

*Department of Chemistry, University of California, Santa Cruz, California 95064*

*Received March 10, 1994; Revised Manuscript Received May 4, 1994®*

ABSTRACT: Intramolecular electron transfer and conformational changes in cytochrome *c* oxidase were studied at room temperature following the photodissociation of CO bound to mixed-valence enzyme (cytochrome $a_3^{2+}$–CO $Cu_B^+$ cytochrome $a^{3+}$ $Cu_A^{2+}$) and fully reduced enzyme. Time-resolved optical absorption difference spectra were collected in the Soret region on time scales of nanoseconds to milliseconds using a gated optical spectrometric multichannel analyzer. A global exponential fitting procedure combined with a singular value decomposition method was used to analyze the transient difference spectra at various times following CO photolysis. The analysis shows that at least two processes, with apparent lifetimes of 1.4 μs and 11.1 ms, are present following the photodissociation of CO bound to the fully reduced enzyme. These are attributed to a conformational change and CO recombination at the cytochrome $a_3$ site, respectively. Global analysis of the mixed-valence CO complex transient difference spectra showed the presence of five intermediates with apparent lifetimes of 1.0 μs, 5.2 μs, 83.7 μs, 10.5 ms, and 25.3 ms. The data on a microsecond time scale are consistent with a mechanism involving a conformational change at cytochrome $a_3$, followed by electron transfer from cytochrome $a_3$ to cytochrome *a* with subsequent electron transfer to $Cu_A$. One of the two processes on a millisecond time scale is attributed to CO recombination and the other to a structural rearrangement or heme–heme electron transfer. On the basis of this mechanism, the kinetics and the absorption spectra of the intermediates involved in the conformational and electron transfer dynamics of the mixed-valence enzyme were determined.

Cytochrome oxidase (CcO;[1] ferrocytochrome *c*:oxygen oxidoreductase, EC 1.9.3.1) of the inner mitochondrial membrane contains at least four redox-active metals, two hemes, cytochrome *a* and cytochrome $a_3$, and two coppers, $Cu_A$ and $Cu_B$, which are involved in the catalysis of electron transfer from cytochrome *c* to dioxygen [see Wikström et al. (1981) for a review]. The enzyme also functions as a proton pump coupled to the electron transfer reactions. A third copper, $Cu_x$, one zinc, and one magnesium atom are also integral to the bovine heart enzyme, but their roles are unknown (Einarsdóttir & Caughey, 1984, 1985; Bombelka et al., 1986; Steffens et al., 1987). Recent spectroscopic evidence suggests that $Cu_A$ may be a mixed-valence dimer, Cu(1.5)---Cu(1.5), in the oxidized enzyme (Kroneck et al., 1989; Scott et al., 1989, 1990; Antholine et al., 1992). It is generally agreed that cytochrome *a* and $Cu_A$ are the primary acceptors of electrons from cytochrome *c*, followed by electron transfer to the dioxygen binding and reduction site, cytochrome $a_3$ and $Cu_B$. However, we do not know the details of the precise electron transfer sequence among the four active redox centers or whether conformational changes accompany the electron transfer processes. Furthermore, the optical absorption spectra of the intermediates involved in the electron transfer are unknown. Elucidation of the factors that control the intramolecular electron transfer processes is essential if we are to understand how they are coupled to proton pumping.

One way to study intramolecular electron transfer in cytochrome oxidase is to photodissociate CO bound to the mixed-valence enzyme (cytochrome $a_3^{2+}$–CO $Cu_B^+$ cytochrome *a* $Cu_A^{2+}$) (Boelens & Wever, 1979; Boelens et al., 1982; Brzezinski & Malmström, 1987; Morgan et al., 1989; Oliveberg & Malmström, 1991; Verkhovsky et al., 1992; Einarsdóttir et al., 1992a; Hallén et al., 1994). Photodissociation of CO from cytochrome $a_3$ lowers the reduction potential of the binuclear site, causing a reversed flow of electrons (relative to the physiological pathway) from the binuclear center, cytochrome $a_3$ and $Cu_B$, to the low-potential redox centers, cytochrome *a* and $Cu_A$ (Boelens & Wever, 1979; Boelens et al., 1982). Oliveberg and Malmström (1991) reported two processes at 445 and 605 nm following the photolysis of CO bound to the mixed-valence enzyme. The two phases, with apparent rates of $2 \times 10^5$ and $1.3 \times 10^4$ $s^{-1}$, were attributed to electron transfer between cytochrome $a_3$ and cytochrome *a* and between cytochrome *a* and $Cu_A$, respectively. Verkhovsky et al. (1992) recently reached similar conclusions when following electron transfer at selected wavelengths in the Soret region. In both studies, non-redox-related events were noted on the same time scale as electron transfer between the two hemes. However, no attempt was made to deconvolute or correct for the spectral changes associated with these events.

In previous studies (Boelens & Wever, 1979; Boelens et al., 1982; Brzezinski & Malmström, 1987; Morgan et al., 1989; Oliveberg & Malmström, 1991; Verkhovsky et al., 1992; Hallén et al., 1994), absorbance changes following the photodissociation of CO from a partially or fully reduced enzyme were followed in a kinetic mode at a single wavelength or a few selected wavelengths using a monochromator/photomultiplier/transient digitizer detection system. As noted

† This work was supported by National Institutes of Health Grant GM45888.

* Author to whom correspondence should be addressed.

® Abstract published in *Advance ACS Abstracts,* July 1, 1994.

[1] Abbreviations: SVD, singular value decomposition; OSMA, optical spectrometric multichannel analyzer; Fe-His, iron–histidine (stretching mode); $E_m$, redox midpoint potential (vs normal hydrogen electrode); $Cu_A$, copper A; $Cu_B$, copper B; $a^{2+}$, reduced cytochrome *a*; $a^{3+}$, oxidized cytochrome *a*; $a_3^{2+}$, reduced cytochrome $a_3$; $a_3^{3+}$, oxidized cytochrome $a_3$; b-spectrum, spectral changes associated with a particular first-order process; CcO, cytochrome oxidase.

0006-2960/94/0433-9245$04.50/0 

earlier (Einarsdóttir et al., 1992a), this mode of detection may lose important information depending on the wavelength(s) selected. Furthermore, the observation of kinetic rates at only a few selected wavelengths does not provide high-resolution absorption spectra of the intermediates involved. In recent studies from our laboratory (Einarsdóttir et al., 1992a), internal electron transfer in cytochrome oxidase was probed on time scales from nanoseconds to milliseconds using a gated optical spectrometric multichannel analyzer (OSMA). This system allowed us to measure optical absorption over a wide spectral range simultaneously and produced high-quality transient difference spectra following the photolysis of CO bound to mixed-valence and fully reduced cytochrome oxidase derivatives (Einarsdóttir et al., 1992a,b).

In this paper, we present extensive Soret region transient absorption difference spectra following photodissociation of CO bound to mixed-valence and fully reduced cytochrome oxidase complexes. The spectra were collected on time scales from 30 ns to 200 ms following CO photolysis and analyzed using a singular value decomposition (SVD) method and a global exponential fitting procedure. This analysis has yielded the kinetics and absorption spectra of the intermediates involved in the CO photodissociation dynamics of mixed-valence and fully reduced cytochrome oxidase complexes.

## MATERIALS AND METHODS

Cytochrome oxidase was isolated from fresh beef hearts according to the method of Yoshikawa et al. (1977). The final precipitate from a fractionation between 25% and 33% ammonium sulfate in 0.5% Tween was dissolved in 0.1 M sodium phosphate buffer (pH 7.4) (no additional detergent added), dialyzed overnight at 4 °C against the same buffer, and stored at −80 °C until further use. Relevant spectroscopic ratios were $A_{444(red)}/A_{420(ox)} = 1.24$ and $A_{604(red)}/A_{598(ox)} = 2.4$. The enzyme concentration was determined using the extinction coefficient of the fully oxidized enzyme at 598 nm or that of the reduced enzyme at 605 nm, 8.5 and 19.9 $mM^{-1}$ $cm^{-1}$, in terms of total heme, respectively (Yoshikawa et al., 1977). The fully reduced enzyme, prepared by the addition of a small excess of dithionite to a deoxygenated enzyme solution, was exposed to CO for 30 min to form the fully reduced CO complex. The mixed-valence CO-bound enzyme was prepared by incubating a deoxygenated enzyme solution under CO for a few hours at room temperature or overnight at 4 °C. The formation of the CO complex was confirmed by its Soret and visible spectra (Greenwood et al., 1974; Morgan et al., 1989).

The CO-bound enzyme complexes were photolyzed with a DCR-11 Nd:YAG laser (532 nm, 45 mJ/pulse). A repetition rate of 2 Hz allowed reformation of the cytochrome $aa_3$–CO complex between pulses. Transient spectral changes initiated by the laser pulse were monitored by a pulsed xenon flash lamp and a gated optical spectrometric multichannel analyzer (OSMA). The time resolution of the probe flash lamp, full width at half-maximum, was 4 μs. The probe flash lamp was powered by a regulated DC power supply, and its energy was low enough that it did not photodissociate the CO complexes. The sample in a 10 × 4 mm cuvet was probed along the 4 mm path length at 90° to the laser photolyzing beam. The probe beam was passed through filters, collimating lenses, the sample, and filters and dispersed by a spectrograph (Aries, FF250) before entering the OSMA detector. The first set of filters was used to block near-UV radiation (<300 nm) and near-infrared radiation (>720 nm), and the second set of filters minimized scattered laser light from entering the spectrograph and maximized the signal-to-noise ratio in the Soret region. The spectrograph with 150 groves/mm grating has a reciprocal linear dispersion of 25.6 nm/mm. The entrance slit width was set at 30 μm. The OSMA detector is a photodiode array (IRY, Princeton Instruments) optically interfaced to a microchannel plate (MCP) intensifier through an optical fiber coupler. It contains 1024 diodes, of which 700 are covered by the intensifier. The OSMA direct memory access controller (PI, ST-120) digitizes the photodiode array channels of the OSMA using a 14-bit analog-to-digital converter.

The time resolution was determined by a pulser (PI, FG-100) with a continuously adjustable gate width from 6 ns to 2.5 μs. To collect a spectrum, the probe flash lamp was triggered, and after a delay of 2 μs the gate pulse was applied, which put it at the maximum of the probe pulse. The time between the probe and the gate pulses was constant during the experiment. To obtain the desired time delay between the laser excitation pulse and the OSMA gate pulse, the probe flash lamp pulse was delayed relative to the Q-switch of the laser. An oscilloscope was used to observe the timing between the pulses. Control of the timing sequences and switching of the mechanized components were accomplished by a 286-12 MHz computer.

Data were collected at 1024 different wavelengths between 215 and 820 nm using an OSMA software program (PI). Values larger than 540 nm and less than 370 nm resulted in excess noise due to low probe intensities and were deleted prior to data analysis. Absorption spectra of both unphotolyzed and photolyzed samples were measured at 38–40 delay times between 30 ns and 200 ms following the laser pulse. Background counts from the detector measured in the absence of the probe and laser photodissociating beams and in the presence of the laser beam alone were also collected. The transient difference spectra (spectra obtained after photolysis minus the spectra collected before photolysis) were obtained by subtracting the background counts and taking the log of corrected probe intensity ratios before and after photolysis. The spectra are averages of 128 scans and have not been smoothed or baseline corrected. The transient difference spectra were analyzed by combining SVD and a global exponential fitting routine that uses a Nelder–Meade simplex algorithm (Hug et al., 1990; Thorgeirsson et al., 1991, 1992) (see below). The analysis was carried out either on a Sun Workstation or on a Macintosh personal computer using Matlab software (The Math Works).

*Spectral Analysis.* The spectral analysis is based upon a matrix formulation of first order kinetics. For any kinetic model involving $N$ intermediates that are connected to each other through a first-order microscopic rate constant, the $N$ differential equations can be expressed in a matrix form by the master equation

$$\dot{\mathbf{c}}(t) = \mathbf{K}\mathbf{c}(t) \tag{1}$$

where $\mathbf{c}(t)$ and $\dot{\mathbf{c}}(t)$ are column vectors containing the concentrations of the intermediates and the corresponding time derivatives, respectively (Haken, 1978). $\mathbf{K}$ is a kinetic matrix, constructed from the microscopic rates connecting the $N$ intermediates and has the form:

$$\begin{bmatrix} -\sum k_{1n} & k_{21} & k_{31} & \dots & k_{N1} \\ k_{12} & -\sum k_{2n} & k_{32} & \dots & k_{N2} \\ \cdot & \cdot & \cdot & \cdot & \cdot \\ \cdot & \cdot & \cdot & \cdot & \cdot \\ \cdot & \cdot & \cdot & \cdot & \cdot \\ k_{1N} & k_{1N} & k_{3N} & \dots & -\sum k_{Nn} \end{bmatrix} \tag{2}$$

where $k_{Nn}$ represents the rate constant for the transition between intermediates $n$ and $N$. The master equation has a solution of the form

$$\mathbf{c}(t) = \exp(\mathbf{K}t)\mathbf{c}(0) \tag{3}$$

where $\mathbf{c}(0)$ is the column vector at time zero. The solution can be written in terms of eigenvectors ($\mathbf{a}_i$) and eigenvalues ($\lambda_i$) of the kinetic matrix, $\mathbf{K}$:

$$\mathbf{c}(t) = \sum f_i \mathbf{a}_i \exp(\lambda_i t) \tag{4}$$

where the constants $f_i$ can be determined from the initial conditions, i.e., the elements of the vector $\mathbf{c}(0)$ (Millhauser & Oswald, 1988).

*Singular Value Decomposition (SVD).* The first step in our spectral analysis involves the application of SVD to the analysis of the transient data (Hug et al., 1990; Thorgeirsson et al., 1991, 1992). The time-resolved difference spectra consist of $\Delta\mathbf{A}(\lambda_m,t_n)$ values, the difference in absorption between the photolyzed and unphotolyzed species, monitored at $m$ wavelengths and $n$ times after photolysis. Therefore, the data can be viewed as an $m \times n$ kinetic two-dimensional matrix, where each of the $m$ rows is a kinetic trace at a single wavelength and each of the $n$ columns represents a difference spectrum at each of the corresponding $n$ times. SVD allows the $\Delta\mathbf{A}$ data matrix ($m \times n$) to be written as a product of three matrices:

$$\Delta\mathbf{A} = \mathbf{USV}' \tag{5}$$

where $\mathbf{U}$ is a matrix ($m \times n$) containing the orthonormal basis spectra, $\mathbf{S}$ is a diagonal matrix ($n \times n$) containing the corresponding eigenvalues, and $\mathbf{V}$ is a matrix ($n \times n$) containing the time evolution of the spectra (Golub & Reinsch, 1970; Henry & Hofrichter, 1992). $\mathbf{V}'$ is the transpose of $\mathbf{V}$. The elements of $\mathbf{S}$ are called singular values ($s_1 > s_2 > s_3 > s_4 \ldots > s_n \geq 0$) and are a quantitative measure of how many linearly independent spectra are needed to reproduce the $\Delta\mathbf{A}$ matrix. The $\Delta\mathbf{A}$ matrix can be represented using a truncated set of basis spectra,

$$\Delta\mathbf{A}_r = \mathbf{US}_r\mathbf{V}' \tag{6}$$

where the new matrix $\mathbf{S}_r$ is truncated by setting $\mathbf{S}_r(ii) = 0$ for all $i > r$. The sum of the squared differences between the actual data and the truncated representation is

$$\sum_{\lambda}\sum_{\text{times}} [\Delta\mathbf{A} - \mathbf{U}_r\mathbf{S}_r\mathbf{V}_r']^2 = \sum_{i>r}^{n} \mathbf{S}_{ii}^2 \tag{7}$$

where the singular values determine the effective rank of the data. When the result of eq 7 is on the order of the noise in the experimental data, the data set is adequately represented by the reduced data set. Typically, only the first few basis spectra are needed to represent the data matrix within the experimental noise. In our case, the first 10 basis spectra ($r = 10$) were used for the subsequent global exponential fitting procedure. In addition to reducing computational time, the SVD analysis provides a quantitative measure of the minimum number of spectrally distinct intermediates present and reduces noise (Golub & Reinsch, 1970; Henry & Hofrichter, 1992). Further details of this analysis are provided elsewhere (Hug et al., 1990; Thorgeirsson et al., 1991; Henry & Hofrichter, 1992).

*Global Exponential Fitting.* Following the SVD analysis, the reduced data set is subjected to global exponential fitting (Hug et al., 1990; Thorgeirsson et al., 1991, 1992). The absorbance changes associated with the time evolution of any first-order interconversions between $N$ intermediates can be described by

$$\Delta\mathbf{A}(\lambda,t) = \sum_{i=0}^{k} \mathbf{b}_i(\lambda) \exp(-k_i t) \tag{8}$$

where $k$ is the number of apparent (observed) rates ($N - 1$), $k_i$ are the apparent (observed) rate constants, and $\mathbf{b}_i(\lambda)$ are the corresponding spectral changes or what we will refer to as b-spectra. Equation 8 can be written in matrix form as

$$\Delta\mathbf{A} = \mathbf{BT} \tag{9}$$

where the $\Delta\mathbf{A}$ matrix is the $m \times n$ data matrix, $\mathbf{B}$ is a matrix ($m \times (k + 1)$) whose columns contain the b-spectra that are associated with the apparent rates, and $\mathbf{T}$ is a $(k + 1) \times n$ matrix whose rows contain the time dependencies of the b-spectra. The exponential fitting program involves the determination of the $\mathbf{B}$ and $\mathbf{T}$ matrices by minimizing the sum of the squared residuals between the fit and the data over all times and wavelengths:

$$\sum_{\lambda}\sum_{\text{times}} [\Delta\mathbf{A} - \mathbf{BT}]^2 = \sum_{i=1}^{m}\sum_{j=1}^{n} [\Delta\mathbf{A}(\lambda_i,t_j) - \sum_{p=0}^{k} \mathbf{b}_p(\lambda_i) \exp(-k_p t_j)]^2 \tag{10}$$

The output of the exponential fitting process is the matrices $\mathbf{B}$ and $\mathbf{T}$, which are related to the eigenvalues and eigenvectors of the kinetic matrix. The apparent rate constants $k_i$ are the eigenvalues of the kinetic matrix with the sign reversed, i.e., $k_i = -\lambda_i$ in eq 4. The b-spectra are related to the eigenvectors of the kinetic matrix through

$$\mathbf{b}_i(\lambda) = \epsilon(\lambda) f_i \mathbf{a}_i \tag{11}$$

where $\epsilon(\lambda)$ is a matrix whose columns contain the spectra of the intermediates, or in our case, the spectra of the intermediates minus the spectrum of the unphotolyzed CO complex since difference spectra rather than absolute spectra are measured.

From eqs 5 and 9,

$$\Delta\mathbf{A} = \mathbf{BT} = \mathbf{USV}' = \mathbf{USCT} \tag{12}$$

where $\mathbf{V}' = \mathbf{CT}$ and $\mathbf{C} = \mathbf{U}^{-1}\mathbf{S}^{-1}\mathbf{B}$. Therefore, instead of fitting the $\Delta\mathbf{A}$ matrix to $\mathbf{BT}$, the $\mathbf{V}'$ matrix is fit to $\mathbf{CT}$. Since the dimensions of $\mathbf{C}$ are $n \times (k + 1)$ and those of $\mathbf{B}$ are $(k + 1) \times m$, this reduction in the dimensions of the matrices greatly reduces the number of linear parameters for the global exponential fitting. In our experiments on the mixed-valence enzyme, the values for $m$, $n$, and $k$ are approximately 300, 40, and 5, respectively. The SVD analysis would therefore reduce the number of linear parameters for the global fitting from 1800 to 240. Using only the first $r$ basis spectra would lead to a further reduction in the number of parameters. With $r = 10$, this number would be $r \times (k + 1)$ or 60 (Hug et al., 1990).

*A Kinetic Mechanism.* The final step in our analysis involves extracting information about the underlying mechanism and the absorption spectra of the intermediates involved. The global fitting procedure using SVD is independent of any specific kinetic mechanism. It gives only information about the apparent variables, i.e., the minimum number of kinetic intermediates, the apparent (observed) rate constants, and the b-spectra from the original transient data. However, the

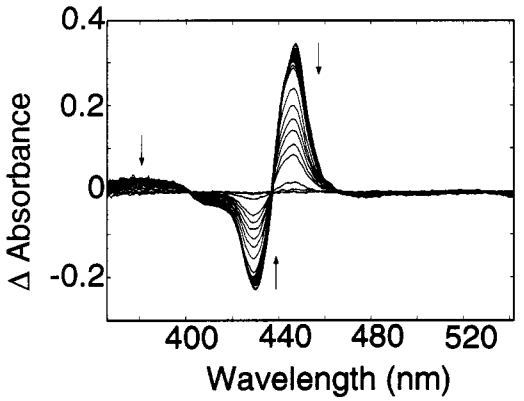


FIGURE 1: Transient absorption difference spectra of fully reduced CO–cytochrome *c* oxidase in the Soret region. The spectra were obtained at 40 delay times between 30 ns and 100 ms after CO photolysis. The number of delay times in each time decade were as follows: 6 between 30 ns and 1 μs, 10 between 1 and 10 μs, 7 between 10 and 100 μs, 6 between 100 μs and 1 ms, 5 between 1 and 10 ms, and 6 between 10–100 ms. Each spectrum represents the average of 128 scans. The cytochrome oxidase concentration was 25 μM in total heme in 0.1 M sodium phosphate buffer (pH 7.4) at 24 °C. The CO concentration was 1 atm.

b-spectra depend both on the difference between the intermediates and the unphotolyzed CO-bound species and on the way the intermediates are interconnected, i.e., the mechanism of the reaction. On the basis of the relationships developed above (eqs 4, 8, and 11), the intermediate spectra and the microscopic rate constants for simple kinetic models can be determined from the b-spectra and the apparent rate constants obtained from the global fitting analysis (Hug et al., 1990; Thorgeirsson et al., 1991, 1992). For a given kinetic scheme, this involves setting up a kinetic matrix in terms of the unknown microscopic rate constants and algebraically finding its eigenvalues. For a simple unidirectional mechanism, the apparent rate constants are equal to the microscopic rate constants, and the determination of the intermediate spectra is straightforward. However, if the kinetic scheme involves back-reaction(s) (as in our case), the number of microscopic rate constants exceeds the number of apparent rates and the kinetic matrix is underdetermined. In these cases, it is necessary to assume one or more of the microscopic rate constants or, alternatively, the equilibrium constants. This has been done in our analysis of the transient difference spectra of the mixed-valence and fully reduced CO complexes. Having obtained the microscopic rate constants, we calculated the intermediate spectra from the kinetic model and the b-spectra (Millhauser & Oswald, 1988). Evaluation of the absorption spectra based on a set of criteria provides validity for the given model.

## RESULTS

*Fully Reduced CO–Cytochrome Oxidase.* Figure 1 shows the transient difference spectra between 30 ns and 200 ms, following the photolysis of CO bound to the fully reduced enzyme. The peak at ~447 nm in the 30 ns difference spectrum corresponds to the photoproduced unliganded cytochrome $a_3^{2+}$, and the trough at ~430 nm corresponds to cytochrome $a_3^{2+}$–CO. The peak at 447 nm is slightly red shifted (1–2 nm) relative to the peak in the ground state difference spectrum of the fully reduced unliganded and the fully reduced CO-bound enzyme (see below). On an early microsecond time scale (30 ns to 10 μs), there is a slight blue shift (~1–2 nm) and a small decrease at 447 nm. This is accompanied by a small bleaching of the trough at 430 nm and a slight increase between 415 and 420 nm. The

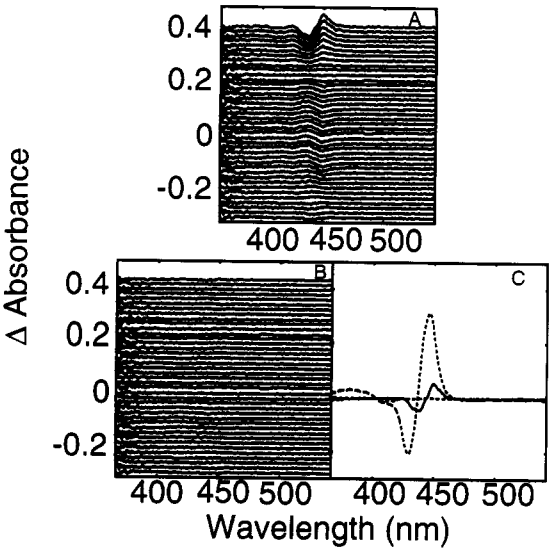


FIGURE 2: Residuals (data minus fit) from one- and two-exponential fits of the time-resolved data of the fully reduced CO complex (Figure 1). The residuals are separated by a constant factor. (A) Residuals for a one-exponential fit ($\tau_{app}$ = 11 ms) and (B) residuals for a two-exponential fit ($\tau_{app}$ = 1.4 μs and 11.1 ms). (C) The spectral changes (b-spectra) associated with the 1.4 μs (—) and 11.1 ms (- - -) lifetimes of the two-exponential fit.

microsecond changes are followed by further bleaching of the peak and the trough on a millisecond time scale, which are attributed to CO recombining with cytochrome $a_3^{2+}$ (Figure 1).

The transient difference spectra were analyzed using SVD and the global exponential fitting procedure to determine the number of intermediates present, the apparent rate constants, and the associated spectral changes, i.e., the b-spectra. The residual spectra obtained assuming one and two processes are compared in Figure 2A,B, respectively. The residuals represent the difference between the transient data and the global fit (eq 10). The residuals based on a single process ($\tau_{app}$ = 11 ms) show a significant positive absorbance on an early microsecond time scale (Figure 2A), which disappears when two exponentials are assumed (Figure 2B). The apparent lifetimes of the two processes were 1.4 μs and 11.1 ms. The associated b-spectra are shown in Figure 2C. It is clear that at least two processes are required to fit the data. The residuals resulting from a two-exponential fit (Figure 2B) show a primarily random structure. However, it was observed that the total residuals were reduced further when the global fit was carried out using three exponentials. Although the small spectral changes associated with the third component were reproduced in different sets of experiments, the apparent lifetime varied (200–400 μs). Therefore, this process was omitted from further analyses. We conclude from the global analysis that the photodissociation cycle of the fully reduced CO-bound complex can be described by at least two kinetic processes. The two apparent lifetimes of 1.4 μs and 11.1 ms are in agreement with our previous studies in which the photolysis of CO bound to the fully reduced enzyme was followed at a few selected wavelengths in the visible region (Einarsdóttir et al., 1993).

*Mixed-Valence CO–Cytochrome c Oxidase.* Figure 3 shows the transient difference spectra following photolysis of CO bound to the mixed-valence enzyme. The peak maximum at ~446 nm and the trough minimum at ~429 nm are slightly blue shifted (1–2 nm) relative to the corresponding values for the fully reduced complex. A substantial absorbance increase occurs between 370 and 420 nm on an early microsecond time

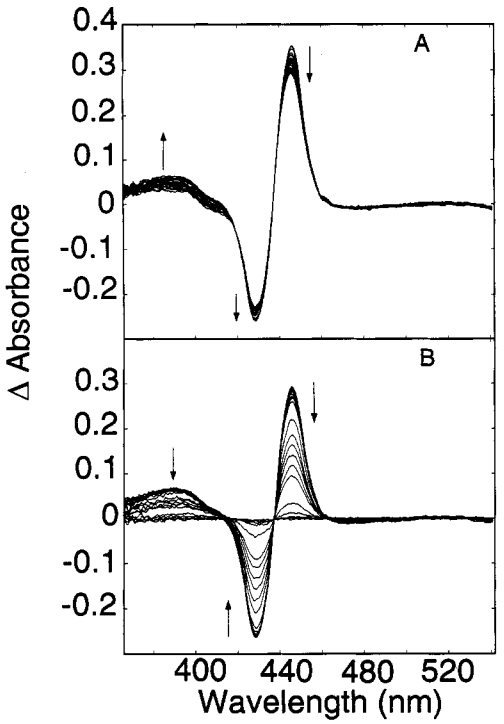


FIGURE 3: Transient absorption difference spectra of mixed-valence CO–cytochrome oxidase between 30 ns and 25 μs (A) and between 25 μs and 200 ms (B) after photolysis of CO from cytochrome $a_3$. The spectra were collected at 38 delay times after the laser pulse with the number of time points in each decade similar to that described in Figure 1. Each spectrum represents the average of 128 scans. Conditions and the concentration of oxidase are the same as in Figure 1.

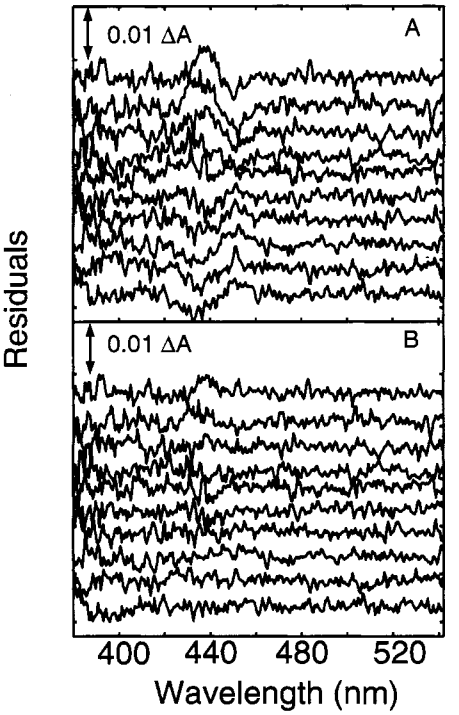


FIGURE 4: Subset of residuals (data minus fit) on a microsecond time scale from (A) a three-exponential fit ($\tau_{app}$ = 2 μs, 43 μs, and 13.5 ms) and (B) a five-exponential fit ($\tau_{app}$ = 1.0 μs, 5.2 μs, 83.7 μs, 10.5 ms and 25.3 ms) of the mixed-valence CO complex transient data (Figure 3). The residuals are separated by a constant factor. Each line (from top to bottom) represents the absorbance difference of the data and the least-squares fit at 1.7, 2, 2.5, 3, 4, 7, 9, 12, 15, and 25 μs after the photodissociation of CO from cytochrome $a_3$.

scale (30 ns to 25 μs) (Figure 3A), accompanied by an increase in the trough at 429 nm and a decrease in the peak at 446 nm. The decrease in the absorbance at 429 nm is most likely due to electron transfer to cytochrome $a^{3+}$, which absorbs at ~426 nm (Vanneste, 1966). This is supported by our spectral analysis in the Discussion. Between 25 and 300 μs after CO photolysis there is a further decrease at 446 nm, with only slight bleaching of the trough at 428 nm. On a millisecond time scale, the transient spectra reflect the recombination of CO with cytochrome $a_3$ (Figure 3B).

SVD analysis of the transient difference spectra in Figure 3A,B showed that the diagonal elements of the S matrix were 8.80, 0.80, 0.123, 0.1146, 0.0653, 0.0574, 0.0523, ... (39 singular values in total). The significant relative magnitudes of the first few singular values indicates that at least three intermediates are present during the CO photodissociation cycle. Following the SVD analysis, the transient difference spectra were fit with different numbers of exponentials (≥3) and the residuals compared. A subset of residuals (1.7–25 μs) from a global fit using three exponentials ($\tau_{app}$ = 2 μs, 43 μs, and 13.5 ms) on the transient difference spectra in Figure 3 (A and B) is shown in Figure 4A. Nonrandomness is clearly seen, suggesting an additional process on a microsecond time scale. Nonrandomness was also observed in a subset of residuals on a millisecond time scale (not shown) when three exponentials were used to fit the transient difference spectra in Figure 3. The systematic structure in the residuals on an early microsecond time scale (as well as on a millisecond time scale) disappears when the data (Figure 3) are analyzed by five kinetic processes (Figure 4B). This suggests that at least five spectrally independent intermediates (excluding the final product, the mixed-valence CO complex) are present in the photodissociation cycle of the mixed-valence CO-bound enzyme. The apparent lifetimes of the five processes were 1.0 μs, 5.2 μs, 83.7 μs, 10.5 ms, and 25.3 ms. The corresponding b-spectra and the total set of residuals are shown in Figure 5. Our earlier SVD and global exponential fitting analysis of transient difference spectra of the mixed-valence CO complex suggested the presence of at least four kinetic processes, with apparent lifetimes of ~100 ns, ~2 μs, ~85 μs, and ~12 ms (Einarsdóttir et al., 1992a). The more extensive data set presented here has permitted us to significantly improve the analysis. These results are in general agreement with recent studies in the visible region, in which five processes with apparent lifetimes similar to those reported here were required to obtain residuals of random structure (Einarsdóttir et al., unpublished results).

The 1 μs apparent lifetime is similar to that observed following the photolysis of CO bound to the fully reduced enzyme. The 5 and 83 μs apparent lifetimes, absent from the fully reduced enzyme, are similar to those reported by Oliveberg and Malmström (1991) and Verkhovsky et al. (1992) for intramolecular electron transfer. On a millisecond time scale, CO recombines with cytochrome $a_3$. A pathway involving both a conformational change and electron transfer on a microsecond time scale will be discussed in detail in the next section.

## DISCUSSION

*Photolysis of the Fully Reduced CO–Cytochrome c Oxidase.* Global analysis of the transient difference spectra of the fully reduced CO–cytochrome oxidase gave two apparent lifetimes. This implies at least two kinetic intermediates in addition to the final product, the fully reduced CO complex. Our previous studies on the photodissociation and recombination dynamics of fully reduced CO-bound cytochrome oxidase

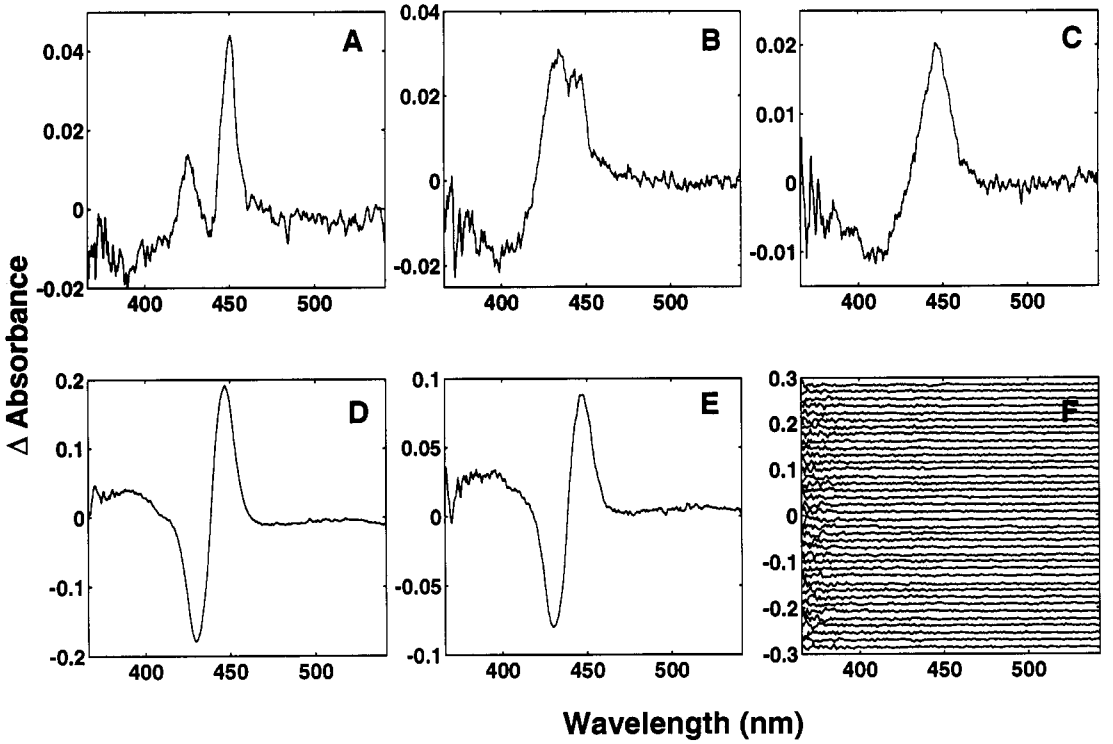


FIGURE 5: (A-E) Spectral changes (b-spectra) from a five-exponential fit to the mixed-valence CO complex transient data (Figure 3). The associated lifetimes were (A) 1.04 μs, (B) 5.21 μs, (C) 83.7 μs, (D) 10.5 ms, and (E) 25.3 ms. (F) The total set of residuals (over all the time points plotted in Figure 3) from the five-exponential fit.

Scheme 1

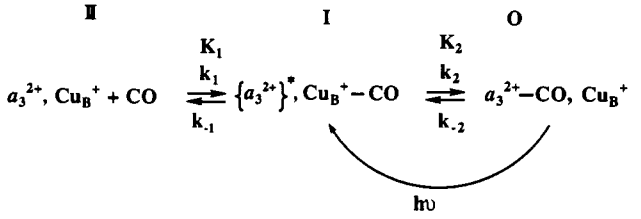


showed that CO binds to $Cu_B$ following the photolysis of CO from cytochrome $a_3$ (Dyer et al., 1989). By following the CO photodissociation and recombination as a function of CO concentration, we also demonstrated that CO binding to cytochrome $a_3$ involves prior binding of CO to $Cu_B^+$ (Woodruff et al., 1991; Einarsdóttir et al., 1993). On the basis of these results, we have used the two-step model in Scheme 1 to determine the absorption difference spectra between the intermediates and the unphotolyzed fully reduced CO species.

Intermediate $\{a_3^{2+}\}^*$, $Cu_B^+$–CO in Scheme 1 represents a transient species in which CO is bound to $Cu_B^+$ and cytochrome $a_3$ is structurally different from the equilibrium species, $a_3^{2+}$,-$Cu_B^+$ (see below). As noted above, to calculate the absorption spectra of intermediates I and II, we require the microscopic rate constants. The equilibrium constant for the first step, $K_1 = k_1/k_{-1}$, is equal to ~90 $M^{-1}$ $s^{-1}$ based on our previous kinetic studies (Woodruff et al., 1991; Einarsdóttir et al., 1993). Since CO is in great excess over the enzyme concentration in our experiments (1 atm of CO ~ 1 mM CO), CO binding to $Cu_B^+$ can be considered pseudo-first-order, a requirement for the exponential fitting analysis. CO recombination is highly favorable in the forward direction [$k_{-2}$ = 0.023–0.027 $s^{-1}$ (Gibson & Greenwood, 1963; Woodruff et al., 1991; Einarsdóttir et al., 1993)] and can, for all practical purposes, be considered unidirectional. On the basis of this information and the apparent rate constants, the microscopic rate constants in Scheme 1 can be determined. These are listed in Table 1 and are in good agreement with our previously determined values (Woodruff et al., 1991; Einarsdóttir et al., 1993).

The intermediate difference spectra (the spectra of the intermediates minus the spectrum of the fully reduced CO complex) in Figure 6A were determined using the mechanism in Scheme 1, the microscopic rate constants (Table 1), and the experimental b-spectra. The absorption spectra of the true intermediates (Figure 6B) were obtained by adding 90% of the spectrum of the fully reduced CO complex (the estimated amount of photolysis) to the intermediate difference spectra in Figure 6A. The correction for 90% photolysis in the

Table 1

| | rate constants | | |
|---|---|---|---|
| | forward | backward | equilibrium constants |
| | Scheme 1 | | |
| fully reduced | $k_1 = 5.9 \times 10^7$ $M^{-1}$ $s^{-1}$ | $k_{-1} = 6.5 \times 10^5$ $s^{-1}$ | $K_1 = k_1/k_{-1} = 90$ $M^{-1}$ |
| | $k_2 = 1.1 \times 10^3$ $s^{-1}$ | $k_{-2} = 0.023$ $s^{-1}$ | $K_2 = 4.8 \times 10^4$ |
| | Scheme 2 | | |
| mixed valence | $k_{1f} = 8.7 \times 10^7$ $M^{-1}$ $s^{-1}$ | $k_{-1r} = 8.7 \times 10^5$ $s^{-1}$ | $K_1' = k_{1f}/k_{1r} = 100$ $M^{-1}$ |
| | $k_{2f} = 1.7 \times 10^5$ $s^{-1}$ | $k_{-2r} = 1.7 \times 10^4$ $s^{-1}$ | $K_{2'} = k_{2f}/k_{2r} = 10$ |
| | $k_{3f} = 1.2 \times 10^4$ $s^{-1}$ | $k_{-3r} = 6.5 \times 10^3$ $s^{-1}$ | $K_3' = k_{3f}/k_{3r} = 1.8$ |
| | $k_{4f} = 9.5 \times 10^2$ $s^{-1}$ | $k_{-4r} = 0.023$ $s^{-1}$ | $K_4' = k_{4f}/k_{4r} = 4.1 \times 10^4$ |

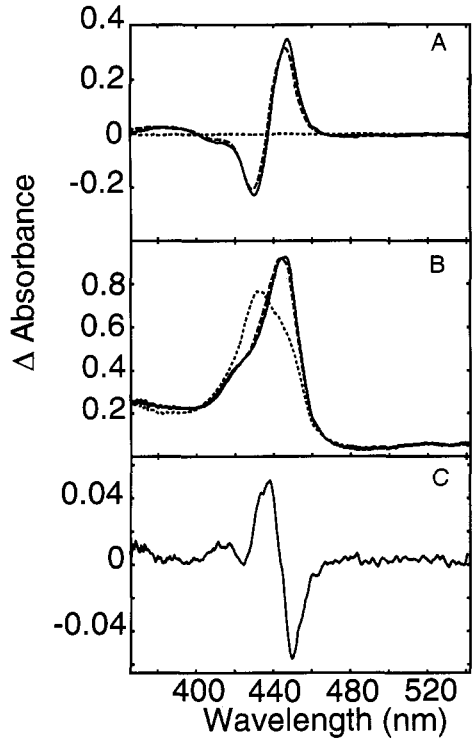


FIGURE 6: (A) Intermediate difference spectra of the fully reduced CO enzyme calculated from the b-spectra in Figure 2C, the mechanism in Scheme 1, and the associated microscopic rate constants (Table 1) (see text). The spectra represent the differences between the intermediates in Scheme 1 and the spectrum obtained before photolysis, i.e., of the fully reduced CO-bound complex. The solid curve represents the intermediate I difference spectrum and the dashed line represents the intermediate II difference spectrum. The dotted line along the baseline represents the intermediate O difference spectrum, i.e., the difference between the final product, the recombined CO complex, and the CO complex before photolysis. (B) The intermediate spectra were obtained by adding 90% (the estimated photolysis yield) of the spectrum of the fully reduced CO-bound complex to the difference spectra in A: intermediate I (—), intermediate II (– –), and intermediate O (- - -). (C) The spectrum of intermediate II minus the spectrum of intermediate I.

transient difference spectra was applied in all future comparisons between the transient and ground state spectra. The intermediate II difference spectrum (Figure 6A, dashed line) is nearly identical to the ground state difference spectrum of the unliganded fully reduced and fully reduced CO-bound cytochrome oxidase, whereas the difference spectrum of intermediate I (Figure 6A, solid line) is slightly red shifted. Correspondingly, the spectrum of intermediate II (Figure 6B, dashed line) is nearly identical to the spectrum of the unliganded fully reduced enzyme at equilibrium. A small red shift was also observed for both cytochrome *b* and $a_3$ bands of the photolyzed $ba_3$ CO-bound oxidase from *Thermus thermophilus* compared with the equilibrium enzyme (Goldbeck et al., 1992). The spectrum of intermediate O in Scheme 1 (Figure 6B, dotted line) is equal to the spectrum of the fully reduced CO-bound enzyme. We conclude that following CO photodissociation and prior to 30 ns, there is a change in the conformation of cytochrome $a_3$, resulting in a red-shifted unliganded phototransient. This species subsequently decays to the unliganded fully reduced state with a rate constant $k_{-1} = 6.5 \times 10^5\ s^{-1}$. The spectral changes associated with the microsecond process, the spectrum of intermediate II minus that of intermediate I, are shown in Figure 6C.

The nature of the conformational change at cytochrome $a_3$ is unknown. This change occurs on the same time scale that CO dissociates from $Cu_B^+$, as shown by time-resolved infrared spectroscopy (Dyer et al., 1989). We have reported spectral changes in the visible region on a picosecond time scale following the photodissociation of CO from cytochrome $a_3$ (Woodruff et al., 1991; Einarsdóttir et al., 1993). These changes were suggested to involve conformational changes at cytochrome $a_3$ triggered by the binding of CO to $Cu_B^+$, which occurs on this time scale (Dyer et al., 1991). Similarly, an absorbance decrease at ~610 nm on a microsecond time scale ($\tau_{app} \sim 1\ \mu s$) was ascribed to the relaxation of the conformational change at cytochrome $a_3$ triggered by the dissociation of CO from $Cu_B^+$ (Woodruff et al., 1991; Einarsdóttir et al., 1993). On the basis of transient optical absorption, time-resolved magnetic circular dichroism and time-resolved resonance Raman data, the conformational change at cytochrome $a_3$ was suggested to involve the transfer of a ligand L from $Cu_B^+$ to cytochrome $a_3$ upon CO binding to $Cu_B^+$ with simultaneous breaking of the proximal histidine bond (Goldbeck et al., 1991; Woodruff et al., 1991; Einarsdóttir et al., 1993). Upon CO dissociation from $Cu_B^+$, ligand L was suggested to return to $Cu_B$ with histidine rebinding at the $a_3$ heme. The rate-limiting step for the CO recombination with cytochrome $a_3$ was suggested to be the dissociation of ligand L. A detailed model incorporating these features has been published previously (Goldbeck et al., 1991; Woodruff et al., 1991; Einarsdóttir et al., 1993).

It should be noted that the picosecond and microsecond processes do not necessarily involve changes in the coordination sphere of the cytochrome $a_3$, but instead may reflect structural changes due to relaxation of the heme pocket. Time-resolved resonance Raman studies on the photodissociation dynamics of the fully reduced CO-bound enzyme have suggested that the cytochrome $a_3$ heme pocket undergoes significant reorganization upon photolysis, with the Fe-His mode evolving from 222 $cm^{-1}$ at 10 ns to its equilibrium position at 214 $cm^{-1}$ on a ~10 $\mu s$ time scale (Findsen et al., 1987; Lou et al., 1993). The shift in the Fe-His mode was suggested to arise from large scale motions of the proximal heme pocket inducing tilt and/or rotation of the proximal histidine.

*Photolysis of the Mixed-Valence CO Complex.* Global analysis of the transient spectra of the mixed-valence CO complex indicates two processes on an early microsecond time scale with apparent lifetimes of ~1 and ~5 $\mu s$. The 1 $\mu s$ lifetime is similar to the lifetime observed following the photolysis of CO bound to the fully reduced enzyme. This suggests that the spectral changes observed in the fully reduced enzyme on a microsecond time scale and attributed to a conformational change at cytochrome $a_3^{2+}$ may also be present in the mixed-valence enzyme. Recent time-resolved infrared experiments have shown that CO binds to $Cu_B^+$ following the photolysis of CO from the mixed-valence enzyme (Woodruff et al., 1993). Time-resolved resonance Raman experiments on the photodissociation dynamics of the mixed-valence CO-bound enzyme have indicated a shift in the Fe-His stretch on a microsecond time scale similar to that observed for the fully reduced enzyme (Lou et al., 1993). Therefore, a conformational change at cytochrome $a_3$ following CO photolysis would also be expected to occur in the mixed-valence enzyme. The 5 $\mu s$ apparent lifetime is similar to the fastest phase observed by Oliveberg and Malmström (1992) at 445 and 605 nm, which they attributed to electron transfer between the two hemes. Our results suggest that two processes, a conformational change at cytochrome $a_3$ and electron transfer between the two hemes, occur in the mixed-valence enzyme on an early microsecond time scale. This is supported by the kinetic modeling in the next section.

Scheme 2

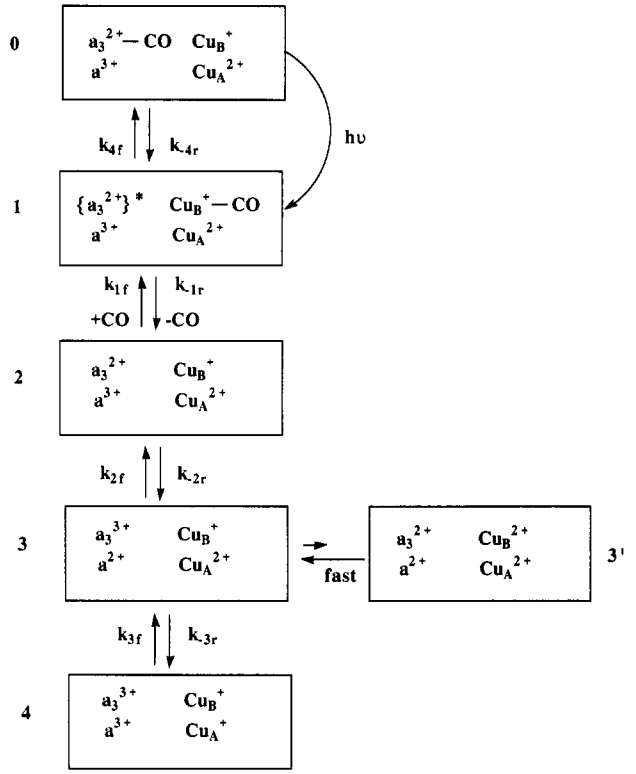


*A Kinetic Model.* The following criteria have been used to construct a model for the CO photodissociation dynamics of the mixed-valence enzyme: (1) the absorbance of all intermediates should be positive at all wavelengths, and (2) the spectra should resemble known spectra of cytochrome oxidase intermediates when available. Using these criteria, we have fit the mixed-valence CO complex time-resolved optical absorption difference spectra (Figure 3) to a sequential pathway that is shown in Scheme 2 with the accompanying equilibria. $k_{1f}$, $k_{2f}$, and $k_{3f}$ represent the rate constants in the forward (physiological) direction, and $k_{1r}$, $k_{2r}$, and $k_{3r}$ represent the rate constants of the reverse processes, i.e., the direction observed in our measurements. The rate constants for CO recombination and thermal dissociation are represented by $k_{4f}$ and $k_{4r}$, respectively. The origin of the second millisecond process is unknown, and it has therefore been omitted from Scheme 2. However, it was included in our spectral analysis (see below).

In Scheme 2, cytochrome $a_3$ is proposed to undergo a structural change following the photodissociation of CO bound to the mixed-valence enzyme. This is accompanied or triggered by CO binding to $Cu_B$, as indicated by the formation of intermediate 1. The structural change at cytochrome $a_3$ may occur on a picosecond time scale, as has been observed for the fully reduced enzyme (Einarsdóttir et al., 1993). It is also conceivable that a simultaneous structural change occurs at cytochrome *a* (see below), although this is not depicted in Scheme 2. The first observable step within our time resolution is postulated to be the return of cytochrome $a_3$ to its equilibrium unliganded state (1 ↔ 2). The second step in Scheme 2, 2 ↔ 3, involves electron transfer between cytochrome $a_3$ and cytochrome *a*. This is followed by electron transfer to $Cu_A$ (3 ↔ 4). In accordance with our previous transient kinetic studies showing that CO binds to $Cu_B^+$ prior to binding to cytochrome $a_3$ (Woodruff et al., 1991; Einarsdóttir et al., 1993), the CO recombination is proposed to originate from intermediate 1 (0 ↔ 1). The second millisecond process could represent a structural change at either heme or, alternatively, electron transfer from cytochrome $a_3$ to cytochrome *a* originating from intermediate 1 rather than intermediate 2. The latter possibility was used in our spectral analysis. Malmström and co-workers recently reported a milliseond process in the internal electron transfer dynamics of the mixed-valence enzyme, which they attributed to electron transfer from cytochrome $a_3$ to cytochrome *a* coupled to proton transfer reactions (Hallén et al., 1994). We do not believe the second millisecond process to be a rate-limiting step for the early microsecond processes. If it were, the amplitudes of the following microsecond processes would be negligible, which they are not. It should be noted that the origin of the second millisecond process, i.e., from which intermediate it branches, does not affect the rate constants (time profiles) or the spectral changes associated with the three short time scale processes, 1 ↔ 2, 2 ↔ 3, and 3 ↔ 4.

*Intermediate Absorbance Spectra.* To determine the spectra of the intermediates postulated in Scheme 2, we need the microscopic rate constants. Since the number of microscopic rate constants exceeds the number of apparent rates, we need to estimate the values of some of the microscopic rate constants. The equilibrium constant for the first step is assumed to be in the same range as that observed for the fully reduced enzyme. The equilibrium constant for the electron transfer between the two hemes is unknown, but it is expected to be highly favored in the physiological direction, i.e., in favor of reduced cytochrome $a_3$ and oxidized cytochrome *a* (Verkhovsky et al., 1992). The equilibrium constant for the third step, $K_3' = k_{3f}/k_{3r}$, is expected to be close to a value of 1.5, determined from the redox potentials of cytochrome *a* and $Cu_A$ in the CO-inhibited enzyme (Ellis et al., 1986; Wang et al., 1986). The values of the equilibrium constants (and, hence, the microscopic constants) were varied until the calculated apparent rates matched the experimental apparent rates and the spectral changes associated with each step resembled those calculated on the basis of Scheme 2 (see below). The values of the microscopic rate constants are listed in Table 1.

The absorption difference spectra between intermediates 1–4 and the unphotolyzed mixed-valence CO complex were derived using the kinetic mechanism in Scheme 2, the observed spectral changes, i.e., the b-spectra, and the microscopic rate constants listed in Table 1 (Figure 7A). The amount of photolysis was assumed to be 90%, as estimated for the fully reduced enzyme. The absorption spectra of the true intermediates in Figure 7B were obtained by adding 90% of the absorption spectrum of the mixed-valence CO complex to the difference spectra in Figure 7A. It is clear that the absorption spectra (Figure 7B) satisfy the criterion that the absorbance of each intermediate is positive at all wavelengths.

Figure 8 shows the time dependence of the populations of intermediates 0–4 during the photodissociation cycle of the mixed-valence CO enzyme based on the model in Scheme 2 and the microscopic rate constants in Table 1. As will be discussed, intermediate 3′ is not significantly populated during the photodissociation cycle and therefore was not included in the kinetic analysis (see following). The time course of the intermediate resulting from the second millisecond process has been omitted.

To determine whether these spectra reflect the expected spectra of the intermediates depicted in Scheme 2, we have compared the spectral differences between successive intermediates to calculated difference spectra determined from the appropriate linear combination of the ground state spectra of oxidized, reduced, mixed-valence CO, and fully reduced

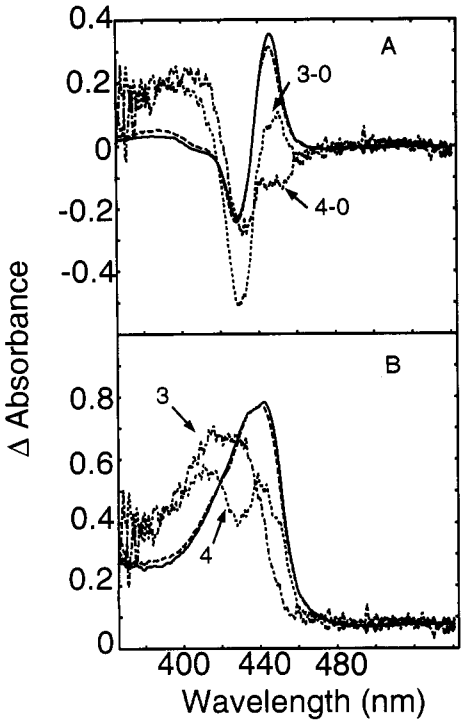


FIGURE 7: (A) Intermediate difference spectra of the mixed-valence CO complex calculated from the b-spectra in Figure 5, the mechanism in Scheme 2, and the associated microscopic rate constants (Table 1) (see text). The spectra represent the differences between the intermediates in Scheme 2 and the mixed-valence CO-bound complex, intermediate O: intermediate 1 (—), intermediate 2 (– –), intermediate 3 (- - -), and intermediate 4 (– - –). (B) The intermediate spectra were obtained by adding 90% of the spectrum of the mixed-valence CO-bound complex to the intermediate difference spectra in A.

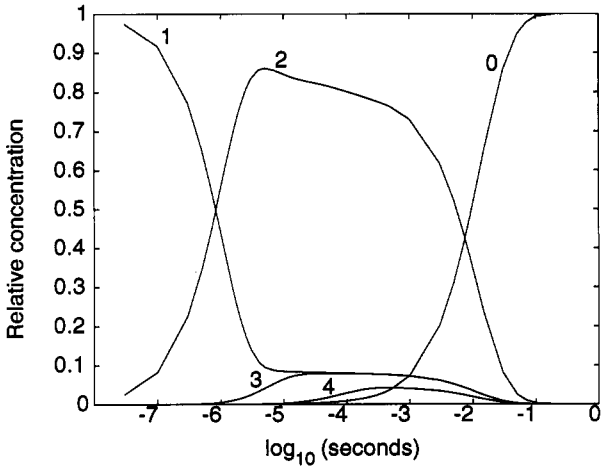


FIGURE 8: Relative concentration–time profiles of the intermediates present during the photodissociation cycle of the mixed-valence enzyme. The time profiles are based on Scheme 2 and the microscopic rate constants in Table 1.

CO enzyme derivatives (Figure 9) (Verkhovsky et al., 1992). The calculated spectra have been corrected for 90% photolysis. As suggested above, the formation of intermediate 1 may involve a structural change at cytochrome $a_3$, possibly triggered by the binding of CO to $Cu_B^+$. Figure 9A shows the spectral change associated with the return of cytochrome $a_3$ to its equilibrium unliganded state (2 minus 1). An equilibrium constant of 100 $M^{-1}$ $s^{-1}$ used for this step represents an upper limit, since a lower value did not significantly alter the difference absorption spectra. The spectral change associated with this process (Figure 9A) is slightly different from the

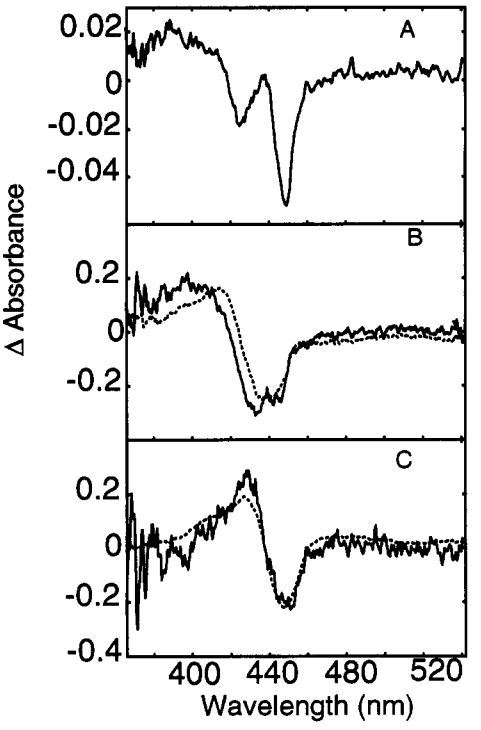


FIGURE 9: (A) Difference between intermediate 2 and intermediate 1 (Scheme 2) in Figure 7. (B and C) Comparison of the spectral differences between successive intermediates in Scheme 2 (—) with the calculated difference spectra (- - -), which were determined from the appropriate linear combination of the ground state absorption spectra of oxidized, reduced, fully reduced CO, and mixed-valence CO enzyme derivatives. The calculated spectra were multiplied by 0.9 to account for 90% photolysis in the experimental spectra. (B) Spectral changes associated with electron transfer between the two hemes. (C) Spectral changes associated with electron transfer between cytochrome *a* and $Cu_A$ (see text for details).

microsecond spectral change observed in the fully reduced enzyme (Figure 6C). The difference between the two is attributed to the effect of the oxidation state of cytochrome *a* and/or $Cu_A$ on the conformational change at the cytochrome $a_3$,$Cu_B$ site. This is supported by recent time-resolved resonance Raman experiments on the CO ligation dynamics of the fully reduced and mixed-valence enzyme complexes (Lou et al., 1993). Alternatively, the conformational change at cytochrome $a_3$ may trigger a simultaneous structural change at cytochrome *a*. Recent structural models based on site-directed mutagenesis studies of cytochrome $aa_3$ of *Rhodobacter sphaeroides* and cytochrome *bo* from *Escherichia coli* indicate that cytochrome *a* and cytochrome $a_3$ are on opposite sides of helix X coordinated by histidines 421 and 419, respectively (Hosler et al., 1993). Due to the close proximity of the two hemes, it is plausible that a structural change at the cytochrome $a_3$ site could trigger spectral changes at cytochrome *a*.

The conformational change is followed by electron transfer between cytochrome $a_3$ and cytochrome *a*. The spectral change (Scheme 2, 3 minus 2) associated with this process, $a^{2+} - a^{3+}$ minus $a_3^{2+} - a_3^{3+}$, is shown in Figure 9B (solid line). Figure 9B (dotted line) also shows the difference between the cytochrome *a*,$Cu_A$ minus cytochrome $a_3$,$Cu_B$ reduced minus oxidized ground state spectra, ($a^{2+}$,$Cu_A^+ - a^{3+}$,$Cu_A^{2+}$) minus ($a_3^{2+}$,$Cu_B^+ - a_3^{3+}$,$Cu_B^{2+}$). This calculated spectrum represents absorbance changes expected for 1:1 electron transfer from cytochrome $a_3$ to cytochrome *a* if spectral interactions and any possible absorbance contribution from the copper centers are neglected. The $a^{2+}$,$Cu_A^+ - a^{3+}$,$Cu_A^{2+}$ spectrum was obtained by subtracting the ground state spectrum of the mixed-valence CO-bound complex from the fully reduced CO

spectrum. It is analogous to spectra obtained using other inhibitors (Vanneste, 1966; Blair et al., 1982). The $a_3^{2+}$,$Cu_B^+$ – $a_3^{3+}$,$Cu_B^{2+}$ spectrum was obtained by subtracting the $a^{2+}$,$Cu_A^+$ – $a^{3+}$,$Cu_A^{2+}$ spectrum from the spectrum of the fully reduced minus oxidized cytochrome oxidase. There is excellent correspondence between the calculated spectrum (Figure 9B, dotted line) and the absorbance changes derived from kinetic modeling (Scheme 2) of the transient data (Figure 3) using the microscopic rate constants in Table 1 (Figure 9B, solid line).

The first electron transfer process is followed by electron transfer to $Cu_A$. The spectral changes associated with this process (Scheme 2, 4 minus 3), $a^{3+}$,$Cu_A^+$ – $a^{2+}$,$Cu_A^{2+}$, are shown in Figure 9C (solid line). Figure 9C (dotted line) also shows the calculated oxidized minus reduced cytochrome $a$,$Cu_A$ difference spectrum, $a^{3+}$,$Cu_A^{2+}$ – $a^{2+}$,$Cu_A^+$, obtained as described above. This difference spectrum should model the electron transfer to $Cu_A$, if one ignores any contribution from the oxidized coppers in this region. Again there is good agreement between the calculated spectrum and the spectrum determined from our kinetic modeling of the transient difference spectra. The equilibrium constant in the photodissociated enzyme ($K_3' = 1.8$) is not significantly different from that measured in the CO-bound enzyme (1.5) (Ellis et al., 1986; Wang et al., 1986). Electron transfer to $Cu_A$ on this time scale is also supported by our near-infrared transient data (Einarsdóttir & Georgiadis, 1992; Einarsdóttir et al., unpublished results), which show an absorbance decrease at 830 nm with an apparent lifetime of ~50–100 μs.

The differences between the experimental and calculated difference spectra in Figure 9B,C are attributed to metal–metal interactions. As noted above, the calculated spectra do not take into account the possible spectral interactions between the two hemes that can arise from the effect of the redox state of one heme on the spectrum of the other or from the effect of ligation at cytochrome $a_3$ on the spectrum of cytochrome $a$. The difference between the experimental and calculated cytochrome $a$ oxidized minus reduced difference spectra in Figure 9C is very similar to differences obtained using various ligands ($CN^-$, NO, and formate) to determine the reduced minus oxidized difference spectrum of cytochrome $a$ (Vanneste, 1966; Blair et al., 1982). These differences were attributed to the effects of the reduction of $Cu_B$ and/or cytochrome $a$ on the extinction of cytochrome $a_3$ (Blair et al., 1982). The other indication of metal–metal spectral interactions is a 1–2 nm blue shift in the 30 ns transient difference spectrum of the mixed-valence CO enzyme (Figure 3) relative to the analogous spectrum of the fully reduced CO complex (Figure 1).

Included in Scheme 2, but omitted from our spectral analysis, is the equilibrium between cytochrome $a_3$ and $Cu_B$ (3 ↔ 3'). A corresponding equilibrium could result from intermediate 4 (not shown). This equilibrium presumably is too fast for our time resolution ($\tau_{app} < 40$ ns). As we have shown above, the spectral changes associated with electron transfer from cytochrome $a_3$ to cytochrome $a$ and between cytochrome $a$ and $Cu_A$ are reasonably well modeled by assuming 1:1 electron transfer between the two hemes and between cytochrome $a$ and $Cu_A$ with no contribution from the equilibrium between cytochrome $a_3$ and $Cu_B$. For this to be true, the equilibrium between cytochrome $a_3$ and $Cu_B$ must lie in favor of the reduction of $Cu_B$ and oxidation of cytochrome $a_3$, as indicated in Scheme 2. This would indicate that the redox midpoint potential of $Cu_B$ must be substantially higher than that of cytochrome $a_3$, as suggested earlier by Verkhovsky et al. (1992).

Our data alone do not allow us to determine whether $Cu_B$ or cytochrome $a_3$ is the electron donor to cytochrome $a$. An equally plausible alternative to Scheme 2 would involve a conformational change at cytochrome $a_3$, subsequent electron transfer from $Cu_B$ to cytochrome $a$, followed by considerably faster electron transfer from cytochrome $a_3$ to $Cu_B$ in favor of the reduction of $Cu_B$. In this case, the electron donated to cytochrome $a$ would originate from $Cu_B$ but appear to be coming from cytochrome $a_3$ (Verkhovsky et al., 1992). In a previous study, we suggested that $Cu_B$ was the electron donor to cytochrome $a$, preceded by a conformational change at cytochrome $a_3$ (Einarsdóttir et al., 1992a). However, recent structural models of the cytochrome $a_3$ and $Cu_B$ binding site place cytochrome $a_3$ between cytochrome $a$ and $Cu_B$ (Hosler, 1993). This arrangement would suggest that the electron donor to cytochrome $a$ is cytochrome $a_3$ and not $Cu_B$. This is supported by recent CO flash photolysis studies on a mixed-valence CO complex of a His333Leu mutant of cytochrome *bo* from *E. coli* lacking $Cu_B$, which show electron transfer on a microsecond time scale, presumably between the two hemes (Brown et al., 1994).

Our apparent lifetimes for intramolecular electron transfer between the two hemes (Table 1) following photolysis of CO from the mixed-valence CO-bound enzyme are in agreement with previous studies. Oliveberg and Malmström (1991) and Verkhovsky et al. (1992) reported an apparent lifetime between 3 and 5 μs for this process. However, in both studies only one apparent rate on an early microsecond time scale was resolved, although a reference was made to non-redox-related changes. We have shown by our global fitting exponential analysis that two early microsecond processes are present and that the absorption spectra of the intermediates can be determined only if both processes are included.

The best fit between the experimental data and the calculated data was obtained using $K_2' = k_{2f}/k_{2r} = 10$ (Table 1) for the electron transfer between the two hemes (Scheme 2). This corresponds to a potential difference of ~60 mV between the $E_m$ values of cytochrome $a_3$ and cytochrome $a$ in intermediates 2 and 3. Similarly, an equilibrium constant of 1.8 between cytochrome $a$ and $Cu_A$ is equivalent to a difference of 15 mV between the $E_m$ values of the cytochrome $a$ and $Cu_A$ in intermediates 3 and 4. Knowledge of the driving force for these steps allows us to calculate the distances between cytochrome $a_3$ and cytochrome $a$ and between cytochrome $a$ and $Cu_A$ on the basis of electron transfer theory as demonstrated by Verkhovsky et al. (1992). Moser and co-workers (Moser & Dutton, 1992; Moser et al., 1992) have shown a log relationship between the optimal rate and the edge-to-edge distance between redox centers in a variety of biological systems. This observation has allowed them to develop an empirical approximation for intraprotein electron transfer, which includes three parameters that modulate the rate of intraprotein electron transfer: distance, free energy, and reorganization energy. Using this relationship, a reorganization energy between 0.7 and 1.0 eV (a range typical for biological electron transfer), and a driving force of 60 mV for the heme–heme electron transfer and 15 mV for the electron transfer from cytochrome $a$ to $Cu_A$, we calculate an edge-to-edge distance of 12–13 Å between the two hemes and a distance of 13–15 Å between cytochrome $a$ and $Cu_A$. The distance of 12–13 Å between the two hemes is similar to the distance of 10.5–12.0 Å reported by Verkhovsky et al. (1992) using the same approach. The edge-to-edge distance of 12–

13 Å is in good agreement with the center-to-center distance range of 12–16 Å between the two hemes (Ohnishi et al., 1982; Mascarenhas et al., 1983; Scholes et al., 1984). A slightly higher value of 20 Å was determined by Brudvig et al. (1984). Distances of 8–13 Å (Goodman & Leigh, 1985) and 13–26 Å (Brudvig et al., 1984) have been reported between cytochrome *a* and $Cu_A$ (Brudvig et al., 1984; Goodman & Leigh, 1985). The short distance between the two hemes is consistent with recent structural models in which the two hemes are ligated to two histidines on opposite sides of helix X, separated by only one residue (Hosler et al., 1993).

## CONCLUSIONS

Global analysis of the mixed-valence CO complex transient data shows that at least five intermediates, in addition to the mixed-valence CO complex, are present in the photodissociation dynamics of the mixed-valence CO complex. On the basis of the mechanism in Scheme 2, we have derived the absorption spectra of intermediates 1–4 (Figure 7) and the corresponding microscopic rate constants (Table 1). The origin of the second millisecond process is under investigation. As indicated in our model, the conformational change at cytochrome $a_3$ and/or the CO dissociation from $Cu_B$ (Scheme 2, 1 ↔ 2) may be prerequisite and rate limiting for the fast electron transfer between cytochrome *a* and cytochrome $a_3$ (Einarsdóttir et al., 1992a). Recent studies by Oliveberg et al. (1992) and Blackmore et al. (1991) have suggested that the pathway for dioxygen to the cytochrome $a_3$ site may be the same as that for CO, namely, prior binding of $O_2$ to $Cu_B^+$. Therefore, the binding of $O_2$ to $Cu_B$ and its subsequent dissociation to bind to cytochrome $a_3$ may involve a structural change at cytochrome $a_3$ similar to what we have observed in the fully reduced enzyme (this study; Woodruff et al., 1991; Einarsdóttir et al., 1993) and the mixed-valence enzyme (this study).

The mechanism in Scheme 2 represents the simplest model to describe the early microsecond conformational and electron transfer dynamics of the mixed-valence enzyme. The good correspondence between the derived absorption spectra of the intermediates and expected spectra provides strong support for the model in Scheme 2. These studies provide additional evidence for $Cu_A$ being the primary acceptor of electrons from cytochrome *c* and cytochrome *a* being the physiological donor of electrons to the dioxygen binding and reduction site (Kobayashi et al., 1989; Hill, 1991; Oliveberg & Malmström, 1991; Pan et al., 1991, 1993; Nilsson, 1992; Verkhovsky et al., 1992). Work currently in progress in our laboratory on the spectral changes occurring in the visible and near-infrared regions following photolysis of CO from the mixed-valence enzyme provides further evidence in support of this model.

## ACKNOWLEDGMENT

We thank Dr. Thorgeir Thorgeirsson for providing programs for the SVD and global exponential fitting analysis and for helpful discussions.

## REFERENCES

Antholine, W. E., Kastrau, D. H. W., Steffens, G. C. M., Buse, G., Zumft, W. G., & Kroneck, P. M. H. (1992) *Eur. J. Biochem. 209*, 875–881.

Blair, D. F., Bocian, D. F., Babcock, G. T., & Chan, S. I. (1982) *Biochemistry 21*, 6928–6935.

Boelens, R., & Wever, R. (1979) *Biochim. Biophys. Acta 547*, 296–310.

Boelens, R., Wever, R., & Van Gelder, B. F. (1982) *Biochim. Biophys. Acta 682*, 264–272.

Bombelka, E., Richter, F.-W., Stroh, A., & Kadenbach, B. (1986) *Biochem. Biophys. Res. Commun. 140*, 1007–1014.

Brown, S., Rumbley, J. N., Moody, A. J., Thomas, J. W., Gennis, R. B., & Rich, P. R. (1994) *Biochim. Biophys. Acta 1183*, 521–532.

Brudvig, G. W., Blair, D. F., & Chan, S. I. (1984) *J. Biol. Chem. 259*, 11001–11009.

Brzezinski, P., & Malmström, B. G. (1987) *Biochim. Biophys. Acta 894*, 29–38.

Dyer, R. B., Einarsdóttir, Ó., Killough, P. M., López-Garriga, J. J., & Woodruff, W. H. (1989) *J. Am. Chem. Soc. 111*, 7657–7659.

Dyer, R. B., Petersen, K. A., Stoutland, P. O., & Woodruff, W. H. (1991) *J. Am. Chem. Soc. 113*, 6276–6277.

Einarsdóttir, Ó., & Caughey, W. S. (1984) *Biochem. Biophys. Res. Commun. 124*, 836–842.

Einarsdóttir, Ó., & Caughey, W. S. (1985) *Biochem. Biophys. Res. Commun. 129*, 840–847.

Einarsdóttir, Ó., Dawes, T. D., & Georgiadis, K. E. (1992a) *Proc. Natl. Acad. Sci. U.S.A. 89*, 6934–6937.

Einarsdóttir, Ó., Georgiadis, K. E., & Dawes, T. D. (1992b) *Biochem. Biophys. Res. Commun. 184*, 1035–1041.

Einarsdóttir, Ó., Dyer, R. B., Lemon, D. D., Killough, P. M., Hubig, S. M., Atherton, S. J., López-Garriga, J. J., Palmer, G., & Woodruff, W. H. (1993) *Biochemistry 32*, 12013–12024.

Ellis, W. R., Jr., Wang, H., Blair, D. F., Gray, H. B., & Chan, S. I. (1986) *Biochemistry 25*, 161–167.

Findsen, E. W., Centeno, J., Babcock, G. T., & Ondrias, M. R. (1987) *J. Am. Chem. Soc. 109*, 5367–5372.

Gibson, Q. H., & Greenwood, C. (1963) *Biochem. J. 86*, 541–554.

Goldbeck, R. A., Dawes, T. D., Einarsdóttir, Ó., Woodruff, W. H., & Kliger, D. S. (1991) *Biophys. J. 60*, 125–134.

Goldbeck, R. A., Einarsdóttir, Ó., Dawes, T. D., O'Connor, D. B., Surerus, K. K., Fee, J. A., & Kliger, D. S. (1992) *Biochemistry 31*, 9376–9387.

Golub, G. H., & Reinsch, C. (1970) *Numer. Math. 14*, 403–420.

Goodman, G., & Leigh, J. S. J. (1985) *Biochemistry 24*, 2310–2317.

Greenwood, C., Wilson, M. T., & Brunori, M. (1974) *Biochem. J. 137*, 205–215.

Haken, H. (1978) *Synergetics*, Springer, New York.

Hallén, S., Brzezinski, P., & Malmström, B. G. (1994) *Biochemistry 33*, 1467–1472.

Henry, E. R., & Hofrichter, J. (1992) *Methods Enzymol. 210*, 129–193.

Hill, B. C. (1991) *J. Biol. Chem. 266*, 2219–2226.

Hosler, J. P., Ferguson-Miller, S., Calhoun, M. W., Thomas, J. W., Hill, J., Lemieux, L., Ma, J., Georgiou, C., Fetter, J., Shapleigh, J., Tecklenburg, M. M. J., Babcock, G. T., & Gennis, R. B. (1993) *J. Bioenerg. Biomembr. 25*, 121–136.

Hug, S. J., Lewis, J. W., Einterz, C. M., Thorgeirsson, T. E., & Kliger, D. S. (1990) *Biochemistry 29*, 1475–1485.

Kobayashi, K., Une, H., & Hayashi, K. (1989) *J. Biol. Chem. 264*, 7976–7980.

Kroneck, P. M. H., Anotholine, W. A., Riester, J., & Zumft, W. G. (1989) *FEBS Lett. 242*, 70–74.

Kroneck, P. M. H., Antholine, W. E., Kastrau, D. H. W., Buse, G., Steffens, G. C. M., & Zumft, W. G. (1990) *FEBS Lett. 268*, 274–276.

Lou, B.-S., Larsen, R. W., Chan, S. I., & Ondrias, M. R. (1993) *J. Am. Chem. Soc. 115*, 403–407.

Mascarenhas, R., Wei, Y.-H., Scholes, C. P., & King, T. E. (1983) *J. Biol. Chem. 258*, 5348–5351.

Millhauser, G. L., & Oswald, R. E. (1988) *Synapse (N.Y.) 2*, 97–103.

Morgan, J. E., Li, P. M., Jang, D.-J., El-Sayed, M. A., & Chan, S. I. (1989) *Biochemistry 28*, 6975–6983.

Moser, C. C., & Dutton, P. L. (1992) *Biochim. Biophys. Acta 1101*, 171–176.

Moser, C. C., Keske, J. M., Warncke, K., Farid, R. S., & Dutton, P. L. (1992) *Nature 355*, 796–802.
Nilsson, T. (1992) *Proc. Natl. Acad. Sci. U.S.A. 89*, 6497–6501.
Ohnishi, T., LoBrutto, R., Salerno, J. C., Bruckner, R. C., & Frey, T. G. (1982) *J. Biol. Chem. 257*, 14821–14825.
Oliveberg, M., & Malmström, B. G. (1991) *Biochemistry 30*, 7053–7057.
Pan, L. P., Hazzard, J. T., Lin, J., Tollin, G., & Chan, S. I. (1991) *J. Am. Chem. Soc. 113*, 5908–5910.
Pan, L. P., Hibdon, S., Liu, R.-Q., Durham, B., & Millet, F. (1993) *Biochemistry 32*, 8492–8498.
Scholes, C. P., Janakiraman, R., Taylor, H., & King, T. K. (1984) *Biophys. J. 45*, 1027–1030.
Scott, R. A., Zumft, W. G., Coyle, C. L., & Dooley, D. M. (1989) *Proc. Natl. Acad. Sci. U.S.A. 86*, 4082–4086.
Steffens, G. C. M., Biewald, R., & Buse, G. (1987) *Eur. J. Biochem. 164*, 295–300.
Thorgeirsson, T. E., Milder, S. J., Miercke, L. J. W., Betlach, M. C., Shand, R. F., Stroud, R. M., & Kliger, D. S. (1991) *Biochemistry 30*, 9133–9142.
Thorgeirsson, T. E., Lewis, J. W., Wallace-Williams, S. E., & Kliger, D. S. (1992) *Photochem. Photobiol. 56*, 1135–1144.
Vanneste, W. H. (1966) *Biochemistry 5*, 838–848.
Verkhovsky, M. I., Morgan, J. E., & Wikström, M. (1992) *Biochemistry 31*, 11860–11863.
Wang, H., Blair, D. F., Ellis, W. R. J., Gray, H. B., & Chan, S. I. (1986) *Biochemistry 25*, 167–172.
Wikström, M., Krab, K., & Saraste, M. (1981) *Cytochrome Oxidase-A Synthesis*, Academic Press, New York.
Woodruff, W. H., Einarsdóttir, Ó., Dyer, R. B., Bagley, K. A., Palmer, G., Atherton, S. J., Goldbeck, R. A., Dawes, T. D., & Kliger, D. S. (1991) *Proc. Natl. Acad. Sci. U.S.A. 88*, 2588–2592.
Woodruff, W. H., Dyer, R. B., & Einarsdóttir, Ó. (1993) in *Biological Spectroscopy, Part B* (Clark, R. J. H., & Hester, R. E., Eds.) pp 189–233, John Wiley and Sons Ltd., Chichester, England.
Yoshikawa, S., Choc, M. G., O'Toole, M. C., & Caughey, W. S. (1977) *J. Biol. Chem. 252*, 5498–5508.